Integrative Biology

A High-Throughput Microtissue Platform to Probe Endothelial Function *In Vitro*

Journal:	*Integrative Biology*
Manuscript ID	IB-TIN-06-2018-000111.R1
Article Type:	Technical Innovation
Date Submitted by the Author:	15-Aug-2018
Complete List of Authors:	Crampton, Alexandra; University of Minnesota, Biomedical Engineering Cummins, Katherine; University of Minnesota, Biomedical Engineering Wood, David; University of Minnesota, Biomedical Engineering

Insight Box

Dysfunction of the endothelial barrier is a hallmark of inflammatory processes and associated with many severe diseases (e.g. atherosclerosis, rheumatoid arthritis, or asthma). The standard measurement of endothelial dysfunction *in vitro* is macromolecular permeability of monolayers grown on transwell inserts. However, transwell platforms overlook physiologically relevant ECM interactions and are severely limited in throughput [ref]. Using endothelial layers cultured on miniaturized collagen microtissues, we created a platform to measure endothelial permeability that alleviates throughput limitations, enhances statistical power, and preserves ECM interactions. As the requirements for number of cells and volume of ECM are minimized, this platform opens up new possibilities for interrogating cell-cell and cell-matrix interactions for high-throughput applications.

A High-Throughput Microtissue Platform to Probe Endothelial Function *In Vitro*

Alexandra L. Crampton[1], Katherine A. Cummins[1], David K. Wood[1]
[1]University of Minnesota, Twin Cities. Department of Biomedical Engineering

Abstract

A critical role of vascular endothelium is as a semi-permeable barrier, dynamically regulating the flux of solutes between blood and the surrounding tissue. Existing platforms that quantify endothelial function *in vitro* are either significantly throughput limited or overlook physiologically relevant extracellular matrix (ECM) interactions and thus do not recapitulate *in vivo* function. Leveraging droplet microfluidics, we developed a scalable platform to measure endothelial function in nanoliter-volume, ECM-based microtissues. In this study, we describe our high-throughput method for fabricating endothelial-coated collagen microtissues that incorporate physiologically relevant cell-ECM interactions. We showed that the endothelial cells had characteristic morphology, expressed tight junction proteins, and remodeled the ECM via compaction and deposition of basement membrane. We also measured macromolecular permeability using two optical modalities, and found the cell layers: (1) had permeability values comparable to *in vivo* measurements and (2) were responsive to physiologically-relevant modulators of endothelial permeability (TNF-α and TGF-β). This is the first demonstration, to the authors' knowledge, of high-throughput assessment (n>150) of endothelial permeability on natural ECM. Additionally, this technology is compatible with standard cell culture equipment (e.g. multi-well plates) and could be scaled up further to be integrated with automated liquid handling systems and automated imaging platforms. Overall, this platform recapitulates the functions of traditional transwell inserts, but extends application to high-throughput studies and introduces new possibilities for interrogating cell-cell and cell-matrix interactions.

Introduction

The vascular system serves crucial roles in supplying nutrients to and removing wastes from peripheral tissues, facilitating immune cell trafficking, and maintaining osmotic homeostasis. These functions depend on the endothelium to act as a semi-permeable barrier between the blood and tissue, which requires the body to regulate and modulate endothelial permeability and thus the flux of cells and/or solutes across the barrier. For example, in inflammatory processes, the endothelial barrier becomes more permeable, facilitating transport of immune cells into the tissue space and inflammatory signals out in order to support the immune response.[1–3] Endothelial barrier function may also be disrupted in disease processes (e.g. atherosclerosis[4–6], rheumatoid arthritis[7–9]), leading to local changes in transport of proteins, fluid volume, and cell populations (including immune cells) into the surrounding tissue. There is also a growing recognition that endothelial barrier function is a critical consideration for delivery of many classes of therapeutics, which can be hindered (e.g. blood-brain barrier[10–14]) or enhanced (e.g. enhanced permeability and retention in solid tumors[15–20]) due to endothelial regulation. Our ability to understand how endothelial barrier function is (dys)regulated in health and disease and how it affects delivery of therapeutics requires robust models of the endothelium and accurate measurement of the barrier function.

One of the standard measurements of endothelial function *in vitro* is macromolecular permeability of monolayers grown on porous transwell inserts.[10,14,21,22] Monolayers are cultured on the insert, and movement of various solutes across the cell layer are typically measured with colorimetric or fluorescently labeled solutes. Although cells attach and consistently form monolayers on these inserts, the endothelial layers are often more leaky than *in vivo* vessels.[21,23–26]. One explanation for the discrpency between *in vitro* and *in vivo* measurements is that the interaction of the endothelium with the tissue compartment is also important for endothelial function. Others probed this hypothesis by coating transwell inserts with ECM molecules[27,28], and found that the exclusion of maromolecular molecules was closer, but still not equivalent to *in vivo* measurements. These findings support the need to create *in vitro* platforms that recapitulate the endothelium in the context of an ECM-rich tissue space. Thus,

there has been significant effort towards developing more physiologically relevant tissue-level models of vasculature *in vitro* using microfluidic devices.[29–32] These models create complex vasculature that directly interacts with ECM and demonstrates characteristic morphology and barrier function. However, the low throughput of these platforms ultimately limits utility for high-throughput screening, revealing a need for an *in vitro* model of the endothelium that is robust, recapitulates the endothelium-ECM interactions in a physiologically meaningful way, and is also amenable to high-throughput studies. Our group[33] and others[34–36] have shown that microcarrier systems can be used to culture endothelial cells, however dynamic measurements of endothelial behavior (e.g. ECM deoposition, changes in endothelial permeability) have yet to be characterized in a high-throughput manner.

Combining the rich cell-ECM interactions of microfluidic platforms and the high-throughput capabilities of droplet technology, we used ECM-based droplets as a substrate for endothelial cells to grow and remodel (via compaction and ECM deposition) – capturing the endothelium-ECM interactions in a format that is compatible with rapid fabricaiton. We demonstrate that microscale (~300 μm diameter) collagen microtissues can be used as ECM-rich carriers on which to culture endothelial cells and can be used to assess factors that regulate endothelial barrier function. These microtissues are fabricated using flow-focusing microfluidic devices, generating ~20,000 droplets/hour, making this ECM-based platform amenable to large-scale studies of endothelial permeability. We show that characteristic behaviors of *in vitro* endothelial layers (confluence of the monolayer, deposition of ECM, and behavior of the semi-permeable barrier) are observed in our microtissue constructs. Additionally, we show for the first time to the authors' knowledge, high-throughput assessment of endothelial function on natural ECM, supporting robust statistical analysis and feasability for large-scale applications. Miniaturization of tissues also minimizes cell number requirements, making this platform amenable to precious cell and ECM sources. We also demonstrate that we can detect biologically relevant modulators of endothelial permeability, using inflammatory cytokines as a sample case.

Experimental

Microtissue Fabrication

Acellular collagen microtissues were fabricated with a modified protocol outlined previously (Figure 1).[33] Briefly, High Concentration Rat Tail Collagen I (Corning) is buffered with 10x PBS, pH adjusted to 7.4, and diluted to a final concentration of 6 mg/mL. At 4°C, the collagen solution was partitioned into microtissues using a flow-focusing microfluidic device. The continuous phase from the droplet generation (FC-40 with 2% EA Surfactant, Ran Biotechnologies), was collected with the collagen microtissues in an eppendorf tube. Microtissues were polymerized in bulk at room temperature for 20 minutes. The oil phase was drained and microtissues were resuspended in 1X sterile PBS.

Microtissue Endothelial Coating

Human Umbilical Vein Endothelial Cells (HUVECs) were cultured in EGM-2 (Lonza) on gelatin-coated flasks. Cells were used between passage 2 and 4 for all experiments. Cells were washed with HBSS and released from the culture flask using 0.05% trypsin (Gibco). Trypsin was neutralized with media, washed with fresh media, and counted. In 12-well low adhesion plates (coated with agarose), 350-500k cells were added to ~750 collagen microtissues. Constructs were cultured in these low-adhesion plates for 5 days, with media changes every 2-3 days. Coated microtissues were recovered from plates with gentle pipetting for experiments.

Crosslinking Collagen Microtissues

Stiffness of collagen microtissues was increased by crosslinking with formalin. Microtissues were incubated with 3.7% formalin for 1 hour at room temperature. Tissues were washed thoroughly with 1X PBS to dilute formalin to <0.001%.

Immunofluorescence Staining

Coated constructs were collected and fixed with 3.7% formalin for at least 1 hour at room temperature. Microtissues were washed with 1X PBS, then quenched with 25 mM glycine. Microtissues were washed, then blocked and permeabilized with 1% BSA and 0.1% Triton X-100. Primary antibodies (VE-Cadherin (Cell Signaling), CD31 (Cell Signaling), Laminin (Abcam), Collagen IV (Abcam)) were diluted in 1% BSA to ratios of 1:100-1:500. Secondary antibodies (Jackson) were diluted in 1% BSA to a ratio of 1:500. Each sample was incubated with 100 uL of antibody solution for either 2 hours at 37°C or overnight at 4°C. Nuclei were labeled with Hoescht (Invitrogen) or Draq5 (Invitrogen).

Permeability Measurement

After culturing microtissues for 5 days, microtissues were collected and placed in a large volume of 12.5 µg/mL 150 kDa TRITC-dextran (Sigma) in a 96-well plate coated with pHEMA (Sigma). Dye diffused into the droplets for 20 minutes before imaging at 10X with the Zeiss Axio Observer. To obtain optical sections, an Apotome was added to the light path and 5 images per slice were collected. Images from both methods were analyzed for local intensity using custom macros written in Fiji.[37] Modulators of permeability were 5 mM EDTA, 10 ng/mL TNF-α (Sigma), 2 ng/mL TGF-β (Sigma).

To calculate permeability from optical sectioning, we assumed the microtissues initially had no fluorescent solute inside the tissue and that all of the solute must pass through the endothelial barrier to reach the center of the tissue. We established an unsteady mass balance where the number of moles of solute on the inside of the tissue was equivalent to the moles of solute that had crossed the endothelial barrier. This was described as:

$$\frac{dC_{drop}}{dt}V_{drop} = A_m P\left(C_{bath} - C_{drop}\right) \quad (1)$$

where C_{drop} was the molar concentration of solute inside the microtissue, V_{drop} was the volume of the microtissue, A_m was the surface area of the microtissue, P was permeability, and C_{bath} was the concentration of the dye bath. As V_{bath} was much greater than V_{drop}, we treated C_{bath} as a constant and simplify Eq. 1:

$$\frac{dC_{drop}}{dt} = \left(\frac{A_m}{V_{drop}}\right) P\left(C_0 - C_{drop}\right) \quad (2).$$

We solved for C_{drop} and applied the initial condition that $C_{drop} = 0$ when t=0. This resulted in the final expression for permeability as:

$$P = -\ln\left(\frac{C_0 - C_{drop}}{C_0}\right)\left(\frac{V_{drop}}{A_m}\right)\left(\frac{1}{t}\right) \quad (3).$$

Additionally, by removing the cell layer using EDTA and calculating permeability of the remodeled ECM, we can identify the contribution of the cell layer and the construct itself separately with:

$$\frac{1}{P_{total}} = \frac{1}{P_{collagen}} + \frac{1}{P_{membrane}} \quad (4).$$

Second Harmonic Imaging to Visualize Collagen Fibers

Second harmonic imaging microscopy was used to visualize collagen fibers in microtissues. Constructs were collected and mounted onto coverslips with 1% agarose. Agarose was chilled to polymerize the gel and the samples were kept hydrated with 1X PBS. Constructs were imaged using a custom multiphoton laser-scanning microscope (Prairie Technologies/Bruker) with a Mai Tai Ti:Sapphire laser (Spectra Physics) exciting fibers at 880 nm. Image intensity within the region of the microtissues were quantified using Fiji.[37]

Statistical Analysis

Large sample sizes allowed for parametric statistical analysis. Comparisons for multiple groups were completed with one-way ANOVA with post-hoc Tukey HSD comparison.[38] Results were reported as statistically significant with p-values less than 0.05.

Results and Discussion

Endothelial Cells Form Confluent Monolayers and Compact ECM Microtissues

It has been previously shown that endothelial cells compact ECM hydrogels *in vitro*[39,40], and we expected that endothelial cells would also compact our collagen microtissues (Figure 1a,b). We further hypothesized that this tissue compaction would result in improved endothelial barrier function. Thus, to compare compacted and uncompacted tissues, we created two types of collagen microtissues. "Soft" microtissues were generated with no post-polymerization modification as described in the Methods. "Stiff" microtissues were generated by crosslinking the polymerized collagen with formalin for 1 hour at room temperature, followed by extensive washing to remove residual fixative. Soft and stiff microtissues were then coated with endothelial cells as described in the Methods.

As shown in Figure 2, endothelial cells formed confluent monolayers on the surface of soft and stiff collagen microtissues. Microtissues were coated with endothelial cells and cultured for up to 5 days, and immunofluorescence was used to assess location and expression of VE-cadherin and CD-31. We used optical sectioning to confirm that cells were on the surface of the microtissues and had characteristic cobblestone morphology (Figure 2a). CD31 and VE-cadherin were detected at the intercellular interfaces of the cells as early as 24 hours after coating (data not shown) as well as 5 days after seeding (Figure 2a). We also measured compaction by the endothelial cells using the projected area of collagen microtissues before and after coating with endothelial cells. We found that the average radius of soft microtissues decreased from 214.68 ± 15.21 μm to 118.66 ±10.32 μm ($p<0.001$) (Figure 2c). As predicted, the average radius of stiff microtisues did not change significantly after coating with cells, with the average radius shifting from 225.28 ± 57.45 μm to 216.45 ± 25.39 μm after 5 days of culture with endothelial cells (Figure 2d). Thus, we confirmed that our platform generates confluent monolayers of endothelial cells that interact with the collagen substrates via adhesion and tissue compaction – both of which are physiolgoically relevant endothelial functions.

Endothelial Cells Anisotropically Remodel Collagen Microtissues

To examine remodeling via compaction in more detail, we used second harmonic generation (SHG) to visualize the collagen architecture throughout the culture process (Figure 3a). We confirmed our finding that soft microtissues were compacted significantly more than stiff microtissues, and that the majority of this compaction was completed within the first 24 hours of culture. We qualitatively observed that the image intensity is brighter for the compacted soft tissues than for the other conditions and quantified this by measuring the average intensity for the entire construct (Figure 3b). The average intensity of the microtissues before and after crosslinking (on day 0) were not statistically different, indicating that the crosslinking process did not affect local collagen distribution or signal from this measurement. We also found that the addition of cells to the stiff microtissues did not change their intensity across any of the days measured (one-way ANOVA, with post-hoc Tukey HSD test). Contrastingly, soft microtissues showed a statistically significant increase in intensity in the first 24 hours after coating ($p<0.01$), and this difference was maintained in all subsequent timepoints (Figure 3b).

Although we observed a dense ring of bright collagen fibers immediately beneath the cell surface (Figure 3a), we wondered if our measured increase in SHG signal intensity was due solely to this dense ring under the cells or if the interior of the microtissue was also affected. To quantify this, we took several linescans from the center to

the edge of the microtissue. We defined a significant increase in intensity to be at least 5 times brighter than the initial measured intensity of acellular constructs (d0). With this, we found that there was little to no remodeling of stiff microtissues in any region of the microtissue. Conversely, the soft microtissues showed significant remodeling deep in the interior of the microtissues, with significant changes in intensity occurring up to 97 μm into the microtissue (Figure 3c).

We found that endothelial cells not only change the diameter of soft microtissues, but also make fundamental changes to the structure of the ECM in the interior of the construct. This predictable pattern of collagen remodeling makes this a simple method for creating dense collagen layers beneath the endothelial layer, which has previously required explicit patterning of ECM.[41] For the stiff constructs, we confirmed that endothelial cells adhere to and interact with the matrix, but were unable to compact the matrix on the local or global scale.

Endothelial Cells Deposit Basement Membrane on Collagen Microtissues

Endothelial cells are known to not only compact ECM hydrogels, but also to deposit basement membrane proteins including collagen IV[42–44], laminin[44], and fibronectin[45] on *in vitro* substrates. To assess this functionality in our platform, we cultured endothelial cells on both soft and stiff microtissues for 5 days. We probed for basement membrane proteins using immunofluorescence and found that endothelial cells deposit collagen IV and laminin on the surface of both soft and stiff microtissues (Figure 2b). This deposition of basement membrane to the surface of the microtissues transforms the plain, isotropic collagen I microtissues into a more physiologically-relevant model of endothelium *in vitro*.

The regulation of basement membrane layers is important in the dynamics of the endothelium. For example, angiogenic processes require degradation of basement membrane before cells can migrate towards an angiogenic signal.[46,47] Thus, the presence of basement membrane in our model system not only supports the existing endothelial layers, but also provides potential for a high-throughput model to study basement membrane dynamics *in vitro*.

Endothelialized Microtissues Demonstrate Permeability Similar to that Observed In Vivo

One of the most important functions of the endothelium is to act as a semi-permeable barrier, dynamically regulating the flux of solutes between blood and the surrounding tissue. The endothelium is selectively permeable, with transport of molecules larger thatn 40-70 kDa excldued very well by healthy endothleium[31,48–50]. We opted to use a tracer comfortably larger than this range (150 kDa) to ensure exclusion by heathy endothelium and to afford more temporal flexibility for our imaging readouts. To assess macromolecular permeability, we examined the flux of 150 kDa TRITC-dextran through soft and stiff microtissues (Figure 4a). To quantify the permeability, we first measured the fluorescence intensity inside and outside of the microtissues. We observed some variability in the absolute intensity of the bath (likely due to photobleaching[51,52]), but we found the difference in intensity between the interior of the microtissue and the surrounding dye bath to be more robust (we report this value as ΔI) (Figure 4b). Using ΔI, we determined that the soft and stiff acellular constructs exhibit similar low impedance to the movement of dye, indicating that the initial stiffness of the construct alone does not affect dye transport for this assay. Both endothelial coated conditions showed a statistically significant increase in ΔI, with the soft-coated condition showing the largest increase in ΔI (Figure 4c). Whether this difference was due to the cell layer, to ECM remodeling, or to both required us to examine the endothelium and the ECM separately. To accomplish this, we removed the cell layer using EDTA, releasing the cells off of the surface of the microtissues and leaving the modified construct behind. We found that the EDTA-treated samples had an intermediate phenotype between the acellular and cellular controls, indicating that the change in ΔI in these microtissues was due to both the impedance from the cell layer and from the remodeling of the constructs. To determine the contribution of each of these

factors, as well as to compare our platform to other macromolecular flux assays, we used the calculated ΔI measurements to determine permeability.

Using an unsteady mass balance, we found the average permeability of the acellular constructs to be 1.09 $x10^{-07}$ ± 5.19 $x10^{-08}$ cm/s and 1.26$x10^{-07}$± 9.26 $x10^{-08}$ cm/s for the soft and stiff microtissues respectively. When a layer of cells is added to these constructs, there is a statistically significant decrease in average permeability to 5.29$x10^{-09}$ ± 1.6 $x10^{-09}$ cm/s and 2.9710^{-08} ± 5.59 $x10^{-09}$ cm/s for the soft and stiff constructs respectively. Once the cell layer is removed using EDTA, we found that the average permeability was 6.56$x10^{-09}$ ± 7.62 $x10^{-10}$ cm/s and 4.98$x10^{-08}$ ± 2.84 $x10^{-08}$ cm/s for the soft and stiff constructs respectively (Figure 4d). For the stiff constructs, this EDTA treatment resulted in a statistically significant increase in permeability, but this effect was not observed for the soft constructs. Using these permeability values to calculate the cellular component with Eq. 4, we found the average permeability of just the cell layer to be 2.75$x10^{-08}$ ± 1.30$x10^{-08}$ cm/s and 7.34$x10^{-08}$ ± 4.19$x10^{-08}$ cm/s for the soft and stiff constructs respectively. Although the total construct permeabilities were very different between the soft and stiff conditions, the contribution of the cell layer alone was on the same order of magnitude.

The measured permeability of our endothelial layers is lower than other reported values for endothelial cells with comparable tracers cultured *in vitro*[21,49] and is comparable to permeabilities reported for vasculature *in vivo*[53,54]. It is well known that ECM interactions improve barrier function *in vitro*[39,42,44,45], and thus we believe the presence of these cell-ECM interactions explain the low permeabilities observed in our constructs. Our endothelial layers (for both the soft and stiff conditions) demonstrated lower permeability values than reported for traditional systems, suggesting that even without the additional resistance to dye movement from compacted tissue, the cell-ECM interactions supported a more *in vivo*-like phenotype. Our soft and stiff constructs demonstrate different transport profiles, which is expected as increasing collagen concentration is known to increase resistance to macromolecular movement within the gels. And thus, our platform is capable of represnting tissue-scale model to study endothelium (soft constructs) as well as an ECM-rich method to examine the endothelium on its own (stiff constructs). This gives us the ability to mimic the *in vivo* environment of endothelium interacting with tissue, but also to observe changes to the endothelium in isolation. Finally, our endothelial constructs demonstrate this lower permeability value in a short culture period of just five days whereas other groups require up to 15 days of culture to obtain comparable results[23]. Our expedient and versatile platform for measuring permeability makes our culture method more amenable to applications in biological discovery and drug screening.

A High-Throughput Assessment of Endothelial Permeability with Widefield Imaging

Quantification of endothelial permeability using optical sectioning affords direct comparison with *in vivo* measurements, but collecting optical sections is significanlty more time-consuming than other modalities, which limits the throughput of the analysis. We hypothesized that by using the ΔI value from widefield images, we could semi-quantitatively assess the permeability of endothelial-coated constructs, which would be appropriate for high throughput studies in which comparison between conditions is more relevant than absolute quantification.

These experiments were conducted similarly to those described for the results in Figure 4. We first implemented a detection scheme that would accommodate a larger population of microtissues (Figure 5a). With the brightfield channel, we used Fiji[37] to threshold the images and bring microtissue constructs to the foreground. We then converted these images to black and white, and used built-in object analysis tools to detect the area, centroid, and edges of each construct. Using the red fluorescence channels, we recorded the intensity across a line from the centroid of the microtissue to 100 pixels outside the edge of the microtissue. We repeated this intensity measurement for a total of 5 linescans per microtissue and averaged the results. This process was automated to expedite the image processing, with a runtime of 1.66 – 7.22 seconds per droplet analyzed. An example of an intensity profile for an endothelial-coated construct is shown (Figure 5a). With widefield imaging, we hypothesized

that the majority of the out-of-plane signal would come from the dye bath above the microtissues. To minimize noise from out-of-plane signal, we also introduced a larger size construct to our experiments, testing the original size (~200 μm radius) and a larger construct (~300 μm radius). We qualitatively observed that the acellular microtissues appeared to be saturated with dye, whereas there was some exclusion of dye with the cell layers for both the endothelial-coated and EDTA-treated conditions (Figure 5b). We calculated the radius of the microtissues (Figure 5c), the average intensity inside and outside of the droplet, and used these values to calculate ΔI for widefield (Figure 5d). The images for each treatment group were collected in 55 seconds, and the average population size examined in this representative dataset is 152 microtissues.

As with our previous experiments, we observed significant changes in the diameters of soft constructs (acellular vs. coated for all conditions $p<0.01$), and observed little to no effect when coating stiff microtissues with endothelial cells (Figure 5c). Next, we examined the transport of 150 kDa TRITC-dextran across the endothelial layer (Figure 5d), which was expected to largely be excluded by a healthy endothelial barrier. For all size and stiffness combinations, we were able to detect a statistically significant change in ΔI between the acellular and coated conditions. This again demonstrates that for all stiffness and size conditions, the addition of the endothelial cell layer created a barrier to solute transport -- either via the cell layer, changes to the ECM, or a combination of the two. Finally, we determined changes in ΔI could be detected with widefield imaging after perturbation of the cell layer by releasing cells with EDTA. We found that with the small, soft condition, we were unable to detect a statistically significant change in ΔI; however, for the large and small stiff constructs as well as the large, soft microtissues, the difference between the coated and EDTA treated conditions were statistically significant ($p<0.01$).

Additionally, endothelial permeability is known to be modulated by cytokines[28,55,56], hormones[57,58], and endotoxins[28,59]. We tested the effect of two inflammatory cytokines – TNF-α and TGF-β – which were expected to increase the flux of dye through the endothelial barrier by disrupting adherens junctions. We found that for both sizes of stiff constructs, there was a statistically significant decrease in ΔI (comparing coated to either TNF-α treated or TGF-β treated, $p<0.01$), meaning that our assay detected the response to the inflammatory cytokines. This change was not observed for either size of the soft constructs, likely due to the additional resistance to diffusion by the compacted ECM. We have shown that using just widefield imaging, we can detect changes in permeability in response to inflammatory signals, using TNF-α and TGF-β for this sample case.

There are several modes of endothelial disruption that are valuable to study *in vitro*. We have shown that the effects of high-concentration chelating agents (e.g. EDTA) can be observed both with optical sectioning and with widefield measurements. This resulted in total physical disruption of the endothelial layer, which could represent a physical injury to the endothelium or could be used to study endothelial healing and remodeling in response to injury in a high-throughput *in vitro* platform. Additionally, lower concentrations or different incubation methods could be used to study physiologically relevant effects of chelating agents, which has applications from studying nitric oxide pathways to optimizing dosing and drug combinations for treating atherosclerosis. We also demonstrated that stimulation with inflammatory cytokines had detectable changes in endothelial permeability. The large sample sizes and ease of fabrication makes this platform well-suited for studying dosing of inflammatory stimuli, as well as screening for vascular toxicity in compound libraries. Finally, as transport across the endothelial barrier is required for all drugs administered intravenously or absorbed through the gastrointestinal tract, this model system could be used to determine the ability of therapeutics to cross the endothelium as a drug screening assay.

Conclusions

Our method for coating ECM-based microtissues with endothelial cells results in endothelium that interacts directly with a collagen tissue compartment – remodeling ECM via compaction as well as deposition of basement membrane proteins. Although others have used microcarries to culture endothelial cells[34–36], we have

demonstrated, for the first time to the authors' knoledge, high-throughput assessment of endothelial permeability on natural ECM, supporting robust statistical analysis. Streamlining our measuremnt furhter, we showed that widefield imaging is a viable method for semi-quantitatively assessing endothelial macromolecular permeability for tissue-level measurments (compacted soft constructs) as well as for just the endothelium (stiff constructs). Changes in dye exclusion were seen in our control conditions (acellular, coated, and EDTA treated); but more importantly, we can use our microtissue platform to detect changes in permeability with physiologically relevant stimuli. With these permeability measurements, we found that our platform recapitulates barrier function that is comparable to in vivo, which we hypothesize is due to the direct coupling of remodeled 3D ECM with the endothelial cell layer.

Our platform enables rapid fabrication (over 20,000 carriers produced per hour), quickly acquires images, and permits automated data analysis of our constructs. The miniaturization of the tissues also minimizes the cell number requirements, making this platform amenable to precious cell and ECM sources. Moreover, because our growth conditions are compatible with standard cell culture equipment (e.g. multi-well plates), this method could be scaled up further and be integrated with automated liquid handling systems and automated imaging platforms. Overall, this platform recapitulates the functions of traditional transwell inserts, but affords novel application to high-throughput studies and opens up new possibilities for interrogating cell-cell and cell-matrix interactions. Permebility assays are not currently used for drug screens as no scalable platforms exist to make this measurement, making our platform an invaluable tool in studying how molecules enter the interstitial space and how they may affect sick or leaky vasculature. Potential applications also include detection of ECM deposition and remodeling in a high-throughput culturing platform, as well as studying specialized endothelial and/or epithelial function in vitro -- including the blood-brain barrier. And due to the increased physiological relevance and the high-throughput nature of microtissues, our platform could facilitate screens for edematous agents or other modulators of endothelial permeability.Additionally, the use of widefield microscopy (as opposed to optical sectioning/confocal) and simple fabrication makes this platform more widely applicable and easier to disseminate to other labs for practical application of this measurement. With the ease of fabrication, flexibility in cell type, and large sample sizes, this platform has a myriad of potential applications.

Conflicts of Interest:
There are no conflicts to declare.

Acknowledgements: We thank the American Heart Association (Scientist Development Grant 13SDG6450000), the National Heart, Lung, and Blood Institute (NHLBI R21 HL132256), the National Institute of Environmental Health Sciences (NIEHS R21 ES027622), the National Science Foundation GRFP (Grant 00039202) for support. Portions of this work were conducted in the Minnesota Nano Center, which is supported by the National Science Foundation through the National Nano Coordinated Infrastructure Network (NNCI) under Award Number ECCS-1542202. We also thank Dr. Paolo Provenzano for the use of his multiphoton microscope, and Julia Nguyen and Dr. Gregory Vercellotti for isolating and generously donating HUVECs.

References

1. Sukriti S, Tauseef M, Yazbeck P, Mehta D. Mechanisms Regulating Endothelial Permeability. Pulm Circ. 2014 Dec 1;4(4):535–51.
2. Sukriti S, Tauseef M, Yazbeck P, Mehta D. Mechanisms regulating endothelial permeability. Pulm Circ. 2014;4(4):535–51.
3. Mantovani A, Bussolino F, Dejana E. Cytokine regulation of endothelial cell function. FASEB J. 1992 May 1;6(8):2591–9.
4. Friedman M, Byers SO. Endothelial permeability in atherosclerosis. Arch Pathol. 1963;76:99–105.

5. Veress B, Bálint A, Kóczé A, Nagy Z, Jellinek H. Increasing aortic permeability by atherogenic diet. Atherosclerosis. 1970 May 1;11(3):369–71.
6. Chatzizisis YS, Umit Coskun A, Jonas M, Edelman ER, Feldman CL, Stone PH. Role of Endothelial Shear Stress in the Natural History of Coronary Atherosclerosis and Vascular Remodeling Molecular, Cellular, and Vascular Behavior. J Am Coll Cardiol. 2007;49(25).
7. Koch AE, Harlow LA, Haines GK, Amento EP, Unemori EN, Wong WL, et al. Vascular endothelial growth factor. A cytokine modulating endothelial function in rheumatoid arthritis. J Immunol. 1994 Apr 15;152(8):4149–56.
8. Koch AE. The role of angiogenesis in rheumatoid arthritis: recent developments. Ann Rheum Dis. 2000 Nov 1;59 Suppl 1(suppl 1):i65-71.
9. Middleton J, Americh L, Gayon R, Julien D, Aguilar L, Amalric F, et al. Endothelial cell phenotypes in the rheumatoid synovium: activated, angiogenic, apoptotic and leaky. Arthritis Res Ther. 2004 Mar 8;6(2):60.
10. Cecchelli R, Dehouck B, Descamps L, Fenart L, Buée-Scherrer V, Duhem C, et al. In vitro model for evaluating drug transport across the blood–brain barrier. Adv Drug Deliv Rev. 1999 Apr 5;36(2–3):165–78.
11. Cecchelli R, Berezowski V, Lundquist S, Culot M, Renftel M, Dehouck M-P, et al. Modelling of the blood–brain barrier in drug discovery and development. Nat Rev Drug Discov. 2007 Aug 1;6(8):650–61.
12. Lockman PR, Koziara JM, Mumper RJ, Allen DD. Nanoparticle Surface Charges Alter Blood–Brain Barrier Integrity and Permeability. J Drug Target. 2004 Dec 3;12(9–10):635–41.
13. Di L, Kerns EH, Fan K, McConnell OJ, Carter GT. High throughput artificial membrane permeability assay for blood–brain barrier. Eur J Med Chem. 2003 Mar 1;38(3):223–32.
14. Hatherell K, Couraud P-O, Romero IA, Weksler B, Pilkington GJ. Development of a three-dimensional, all-human in vitro model of the blood–brain barrier using mono-, co-, and tri-cultivation Transwell models. J Neurosci Methods. 2011 Aug 15;199(2):223–9.
15. Dreher MR, Liu W, Michelich CR, Dewhirst MW, Yuan F, Chilkoti A. Tumor Vascular Permeability, Accumulation, and Penetration of Macromolecular Drug Carriers. JNCI J Natl Cancer Inst. 2006 Mar 1;98(5):335–44.
16. Greish K. Enhanced permeability and retention of macromolecular drugs in solid tumors: A royal gate for targeted anticancer nanomedicines. J Drug Target. 2007 Jan 8;15(7–8):457–64.
17. Yuan F, Leunig M, Huang SK, Berk DA, Papahadjopoulos D, Jain RK. Microvascular permeability and interstitial penetration of sterically stabilized (stealth) liposomes in a human tumor xenograft. Cancer Res. 1994 Jul 1;54(13):3352–6.
18. Iyer AK, Khaled G, Fang J, Maeda H. Exploiting the enhanced permeability and retention effect for tumor targeting. Drug Discov Today. 2006 Sep 1;11(17–18):812–8.
19. Danhier F, Feron O, Préat V. To exploit the tumor microenvironment: Passive and active tumor targeting of nanocarriers for anti-cancer drug delivery. J Control Release. 2010 Dec 1;148(2):135–46.
20. Tozer GM, Kanthou C, Baguley BC. Disrupting tumour blood vessels. Nat Rev Cancer. 2005 Jun 1;5(6):423–35.
21. Siflinger-Birnboim A, del Vecchio PJ, Cooper JA, Blumenstock FA, Shepard JM, Malik AB. Molecular sieving characteristics of the cultured endothelial monolayer. J Cell Physiol. 1987 Jul 1;132(1):111–7.
22. Maruo N, Morita I, Shirao M, Murota S. IL-6 increases endothelial permeability in vitro. Endocrinology. 1992 Aug 1;131(2):710–4.
23. Casnocha SA, Eskin SG, Hall ER, McIntire L V. Permeability of human endothelial monolayers: effect of vasoactive agonists and cAMP. J Appl Physiol. 1989 Nov;67(5):1997–2005.
24. Bratzler RL, Chisolm GM, Colton CK, Smith KA, Lees RS. The distribution of labeled low-density lipoproteins across the rabbit thoracic aorta in vivo. Atherosclerosis. 1977 Nov 1;28(3):289–307.
25. Ma X, Zhang H, Pan Q, Zhao Y, Chen J, Zhao B, et al. Hypoxia/Aglycemia-Induced Endothelial Barrier Dysfunction and Tight Junction Protein Downregulation Can Be Ameliorated by Citicoline. Tang YL, editor. PLoS One. 2013 Dec 16;8(12):e82604.
26. Kevil CG, Payne DK, Mire E, Alexander JS. Vascular permeability factor/vascular endothelial cell growth factor-mediated permeability occurs through disorganization of endothelial junctional proteins. J Biol Chem. 1998 Jun 12;273(24):15099–103.

27. Nooteboom A, Hendriks T, Ottehöller I, van der Linden CJ. Permeability characteristics of human endothelial monolayers seeded on different extracellular matrix proteins. Mediators Inflamm. 2000;9(5):235–41.
28. Nooteboom A, Van Der Linden CJ, Hendriks T. Tumor necrosis factor-alpha and interleukin-1beta mediate endothelial permeability induced by lipopolysaccharide-stimulated whole blood. Crit Care Med. 2002;30(9):2063–8.
29. Zervantonakis IK, Hughes-Alford SK, Charest JL, Condeelis JS, Gertler FB, Kamm RD. Three-dimensional microfluidic model for tumor cell intravasation and endothelial barrier function. Proc Natl Acad Sci. 2012;109(34):13515–20.
30. Jeon JS, Bersini S, Whisler JA, Chen MB, Dubini G, Charest JL, et al. Generation of 3D functional microvascular networks with human mesenchymal stem cells in microfluidic systems. Integr Biol. 2014 Apr 22;6(5):555–63.
31. Moya ML, Hsu Y-H, Lee AP, Hughes CCW, George SC. *In Vitro* Perfused Human Capillary Networks. Tissue Eng Part C Methods. 2013;19(9):730–7.
32. Mannino RG, Santiago-Miranda AN, Pradhan P, Qiu Y, Mejias JC, Neelapu SS, et al. 3D microvascular model recapitulates the diffuse large B-cell lymphoma tumor microenvironment in vitro. Lab Chip. 2017 Jan 31;17(3):407–14.
33. Brett M-E, Crampton AL, Wood DK. Rapid generation of collagen-based microtissues to study cell–matrix interactions. TECHNOLOGY. 2016 Jun 26;04(02):80–7.
34. Gryglewski RJ, Moncada S, Palmer RMJ. Bioassay of prostacyclin and endothelium-derived relaxing factor (EDRF) from porcine aortic endothelial cells. Br J Pharmacol. 1986 May 1;87(4):685–94.
35. Feng X, Tonnesen MG, Mousa SA, Clark RAF. Fibrin and Collagen Differentially but Synergistically Regulate Sprout Angiogenesis of Human Dermal Microvascular Endothelial Cells in 3-Dimensional Matrix. Int J Cell Biol. 2013;2013:1–11.
36. Matsunaga YT, Morimoto Y, Takeuchi S, Matsunaga YT, Morimoto] Y, Takeuchi † S, et al. Molding Cell Beads for Rapid Construction of Macroscopic 3D Tissue Architecture. Adv Mater. 2011;23:90–4.
37. Schindelin J, Arganda-Carreras I, Frise E, Kaynig V, Longair M, Pietzsch T, et al. Fiji: an open-source platform for biological-image analysis. Nat Methods. 2012 Jul 1;9(7):676–82.
38. Kramer CY. Extension of Multiple Range Tests to Group Means with Unequal Numbers of Replications. Biometrics. 1956 Sep;12(3):307.
39. Liu XD, Skold M, Umino T, Zhu YK, Romberger DJ, Spurzem JR, et al. Endothelial cell–mediated type I collagen gel contraction is regulated by hemin. J Lab Clin Med. 2000 Aug 1;136(2):100–9.
40. Stevenson MD, Sieminski AL, McLeod CM, Byfield FJ, Barocas VH, Gooch KJ. Pericellular Conditions Regulate Extent of Cell-Mediated Compaction of Collagen Gels. Biophys J. 2010 Jul 7;99(1):19–28.
41. Han S, Shin Y, Jeong HE, Jeon JS, Kamm RD, Huh D, et al. Constructive remodeling of a synthetic endothelial extracellular matrix. Sci Rep. 2016 Nov 21;5(1):18290.
42. Jaffe EA, Minick CR, Adelman B, Becker CG, Nachman R. Synthesis of basement membrane collagen by cultured human endothelial cells. J Exp Med. 1976 Jul 1;144(1):209–25.
43. Kramer RH, Fuh GM, Karasek M a. Type IV collagen synthesis by cultured human microvascular endothelial cells and its deposition into the subendothelial basement membrane. Biochemistry. 1985;24(25):7423–30.
44. Kramer RH, Bensch KG, Davison PM, Karasek MA. Basal lamina formation by cultured microvascular endothelial cells. J Cell Biol. 1984 Aug 1;99(2):692–8.
45. Jaffe EA, Mosher DF. Synthesis of fibronectin by cultured human endothelial cells. J Exp Med. 1978 Jun 1;147(6):1779–91.
46. Nguyen M, Arkell J, Jackson CJ. Human endothelial gelatinases and angiogenesis. Int J Biochem Cell Biol. 2001 Oct 1;33(10):960–70.
47. Chang C, Werb Z. The many faces of metalloproteases: cell growth, invasion, angiogenesis and metastasis. Trends Cell Biol. 2001 Nov 1;11:S37–43.
48. Egawa G, Nakamizo S, Natsuaki Y, Doi H, Miyachi Y, Kabashima K. Intravital analysis of vascular permeability in mice using two-photon microscopy. Sci Rep. 2013;3:1932.

49. Van Duinen V, Van Den Heuvel A, Trietsch SJ, Lanz HL, Van Gils JM, Van Zonneveld AJ, et al. 96 perfusable blood vessels to study vascular permeability in vitro. Sci Rep. 2017;7:18071.
50. Faraci FM, Choi J, Baumbach GL, Mayhan WG, Heistad DD. Microcirculation of the Area Postrema Permeability and Vascular Responses.
51. Burns A, Ow H, Wiesner U. Fluorescent core–shell silica nanoparticles: towards "Lab on a Particle" architectures for nanobiotechnology. Chem Soc Rev. 2006 Oct 23;35(11):1028–42.
52. Real-Hohn A, Zancan P, Da Silva D, Martins ER, Salgado LT, Mermelstein CS, et al. Filamentous actin and its associated binding proteins are the stimulatory site for 6-phosphofructo-1-kinase association within the membrane of human erythrocytes. Biochimie. 2010 May 1;92(5):538–44.
53. Yuan F, Dellian M, Fukumura D, Leunig M, Berk DA, Torchilin VP, et al. Vascular Permeability in a Human Tumor Xenograft: Molecular Size Dependence and Cutoff Size1. Vol. 55, CANCER RESEARCH. 1995.
54. Rizzo V, Kim D, Durán WN, DeFouw DO. Ontogeny of Microvascular Permeability to Macromolecules in the Chick Chorioallantoic Membrane during Normal Angiogenesis. Microvasc Res. 1995 Jan 1;49(1):49–63.
55. Marcos-Ramiro B, García-Weber D, Millán J. TNF-induced endothelial barrier disruption: beyond actin and Rho. Thromb Haemost. 2014 Nov 20;112(12):1088–102.
56. Connolly DT, Heuvelman DM, Nelson R, Olander J V, Eppley BL, Delfino JJ, et al. Tumor vascular permeability factor stimulates endothelial cell growth and angiogenesis. J Clin Invest. 1989 Nov 1;84(5):1470–8.
57. Naomasa N, Norio N, Shoso Y. The effect of histamine on cultured endothelial cells A study of the mechanism of increased vascular permeability. Eur J Pharmacol. 1992 Oct 20;221(2–3):325–31.
58. van Nieuw Amerongen GP, Draijer R, Vermeer MA, Van Hinsbergh VWM. Transient and Prolonged Increase in Endothelial Permeability Induced by Histamine and Thrombin Role of Protein Kinases, Calcium, and RhoA. 1998.
59. Harlan JM, Harker LA, Reidy MA, Gajdusek CM, Schwartz SM, Striker GE. Lipopolysaccharide-mediated bovine endothelial cell injury in vitro. Lab Invest. 1983 Mar;48(3):269–74.

Figures

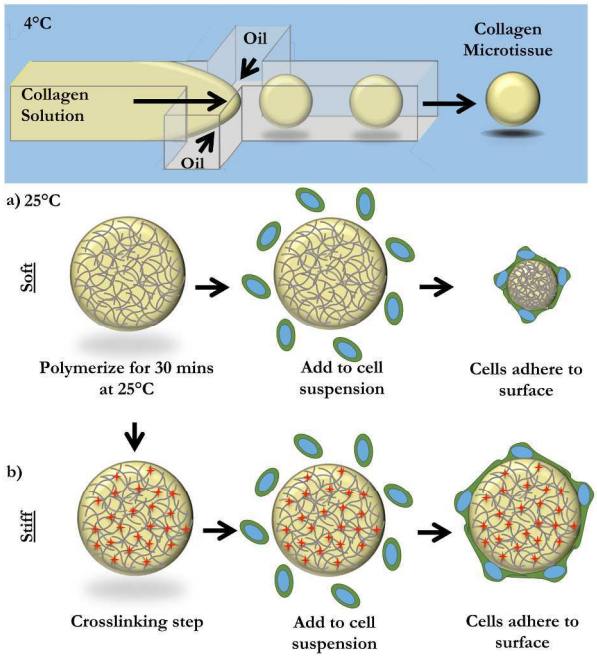

Figure 1: Fabrication of Endothelial-coated Collagen Microtissues. Liquid 6 mg/mL collagen I microtissues were generated using a chilled flow-focusing microfluidic device. Microtissues were collected and polymerized off-chip at 25°C for 30 minutes. (a) In the case of "soft" microtissues, we did not need to further manipulate the collagen microtissues. To coat with cells, microtissues were mixed with a single-cell suspension of endothelial cells. In this "soft" mode, cells compacted the collagen microtissues. (b) To prevent compaction, we created "stiff" microtissues. After polymerization, microtissues were crosslinked with formalin. "Stiff" microtissues were then washed thoroughly and coated by incubating with a single cell suspension of endothelial cells. Cells created a monolayer on the surface of the microtissues, but did not change the overall size of these "stiff" microtissues.

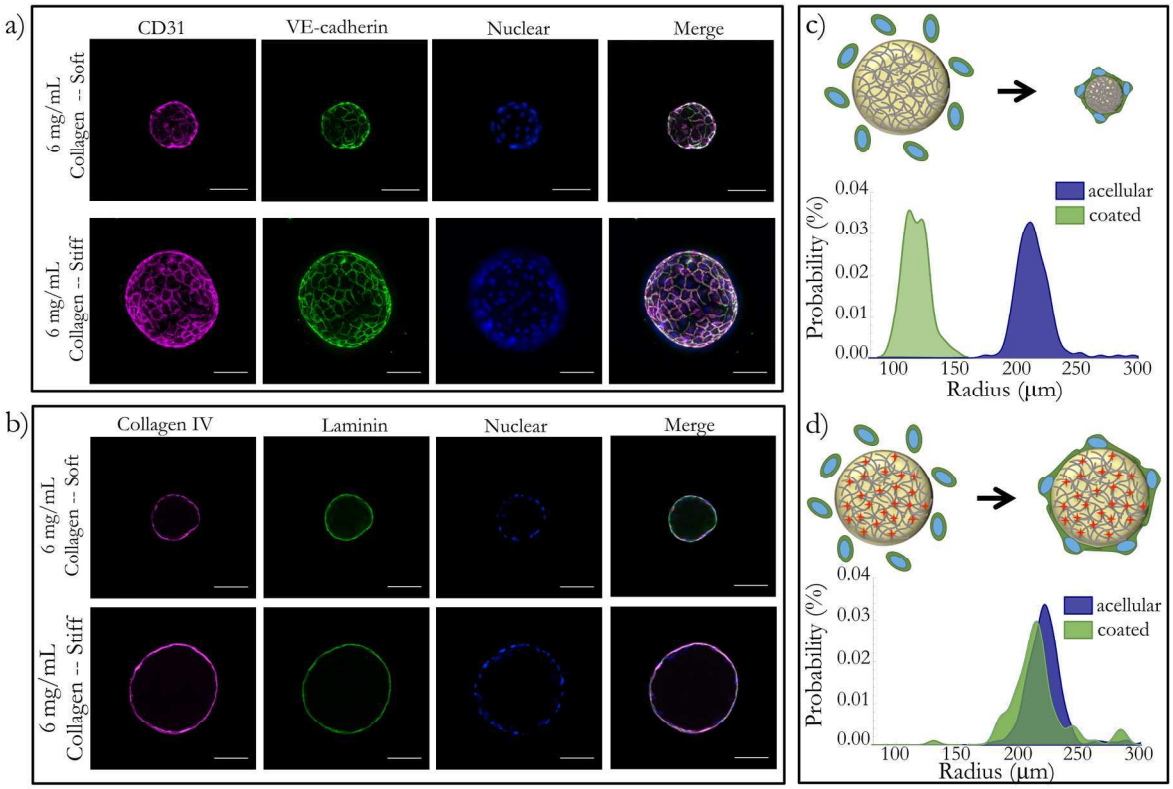

Figure 2: Endothelial cells formed confluent monolayers and remodel ECM-based microtissues. Both soft and stiff microtissues were coated with endothelial cells and cultured for 5 days. (a) On both soft and stiff microtissues, cells create confluent monolayers. Cells in all conditions have characteristic morphology and tight-junction expression, visualized with CD31 and VE-cadherin. (b) Using immunofluorescence, we observed that the endothelial cells deposited Collagen IV and Laminin on the surface of the collagen constructs for both the soft and stiff conditions. We qualitatively observed that (c) coating soft matrices with endothelial cells resulted in compaction, but (d) stiff matrices did not have a significant size change. We quantified the projected area of the droplets before and after coating to quantify this result and found the population shift for the compaction to be extremely statistically significant, but observed no statistically significant change for the stiff matrices. Scale bars 100 μm.

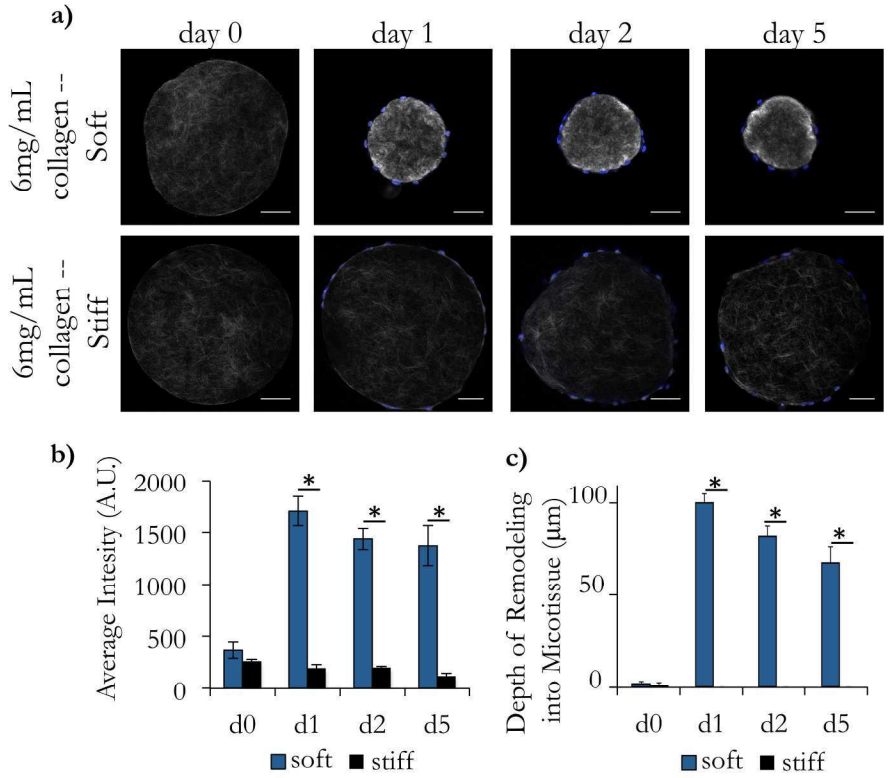

Figure 3: Second harmonic generation imaging reveals local remodeling of collagen architecture. Acellular collagen droplets were coated with endothelial cells and cultured for 5 days. (a) At intermediate timepoints, droplets were collected and imaged using Second Harmonic Generation (SHG) to visualize the collagen fibers. (b) We observed that the average intensity of the soft microtissues on d1, d2, and d5 after coating with endothelial cells was significantly higher than acellular as well as the corresponding timepoints for the stiff tissues. In (a), we observed a dense ring of collagen at the surface of the microtissues. (c) To quantify this, we took linescans from the center of the microtissues to the surface and recorded the image intensity along the line. We repeated this 5 times for each droplet and reported a moving average with standard error of these linescans for each condition. (d) Using these intensity profiles, we measured the distance into the droplet that displayed large differences in intensity (defined as 5-fold brighter than the baseline average on the d0 measurements). We found that the stiff droplets showed very little remodeling of the interior of the droplet, but the soft constructs had large changes in intensity up to 97 μm from the surface of the droplet. Scale bars 100 μm.

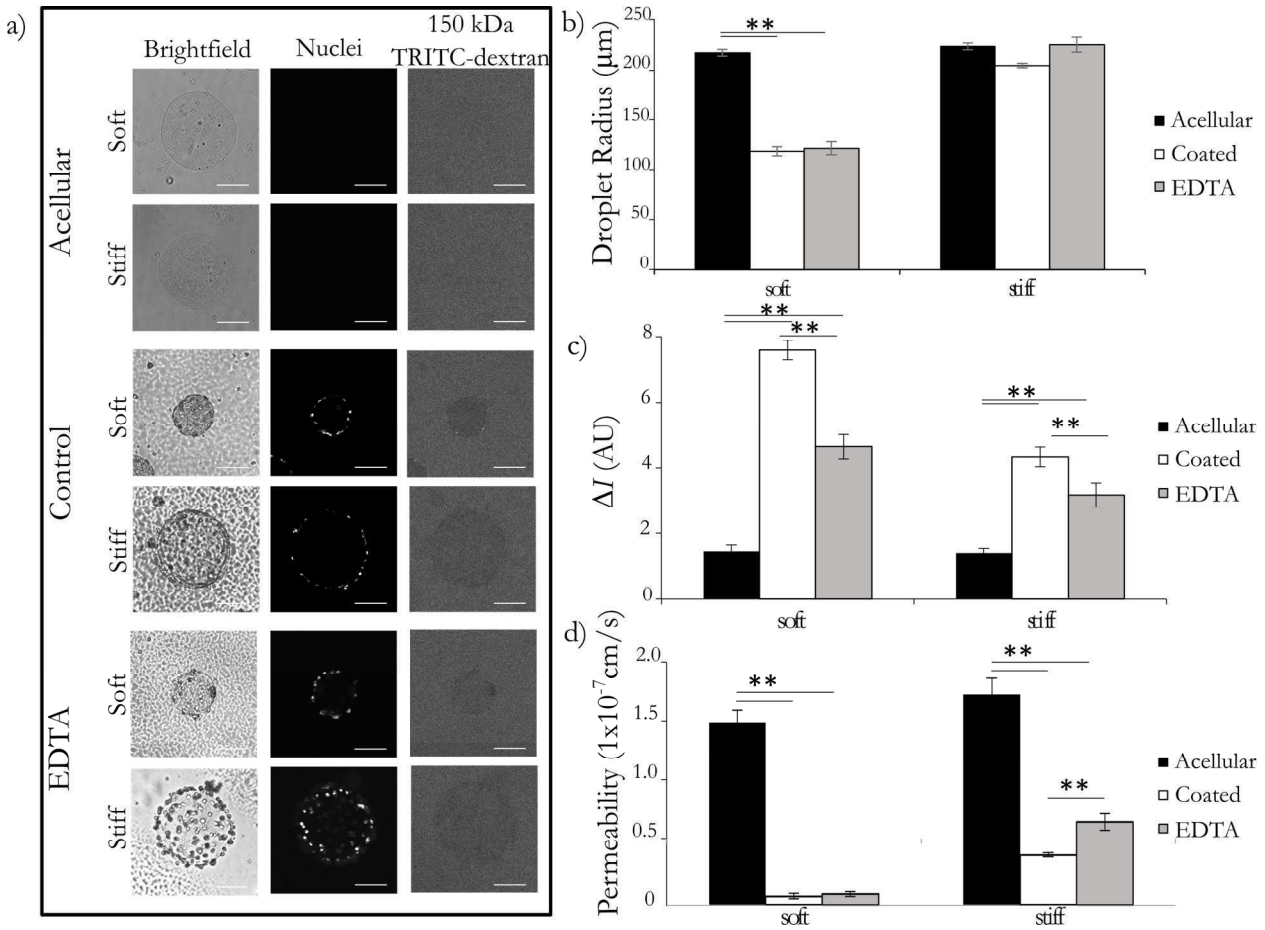

Figure 4: Microtissue endothelial barrier function is comparable to in vivo *permeability.* Endothelial cells were cultured on the surface of soft and stiff collagen microtissues for 5 days. Tissues were collected and some were treated with 5mM EDTA for 30 minutes. Constructs were placed in a 12.5 ug/mL dye bath and incubated for 20 minutes. (a) Constructs were imaged with brightfield and optical sectioning. Brightfield imaging shows the location and geometry of the microtissues, nucelear stain confirms the presence of ceslls, and the movement 150kDa TRITC-Dextran was visualized with flourescence microscopy. We qualitatively observe that acellular constructs do not impede dye movement, whereas the control condition showed exclusion of the dye from the interior of the microtissue for both the soft and stiff conditions. The EDTA treated condition appeared to have an intermediated phenotype. Backround noise was reduced in representative images for clarity. (b) We report the average droplet radius with standard error, showing that the soft constructs were compacted significantly, and the stiff constructs were largely unchanged in diameter. (c) Comparing the intensity inside and outside the droplet (ΔI), we found that ΔI was small for acellular constructs, and largest for coated constructs for both soft and stiff microtissues. We found that the removal of the cell layer resulted in an intermediate ΔI for both stiffnesses. (d) Converting the ΔI to the permeability using Eq. (3), we found the acellular constructs to have the largest permeability, and the coated controls to have a permeability that was statistically significantly smaller for both cases. For the EDTA treated group, we found that this increased the average permeability for the stiff constructs in a statistically significant manner. There was a slight increase in the average also for the soft constructs, but this difference was not statistically significant. We used these permeability values to calculate the contribution of the ECM and the cell layers individually and found the permeability of the cell layer to be on the order of $1x10^{-8}$ cm/s. assay. All comparisons completed with one-way ANOVA with post-hoc Tukey HSD test; $p<0.01$ = **. Scale bars 100 μm.

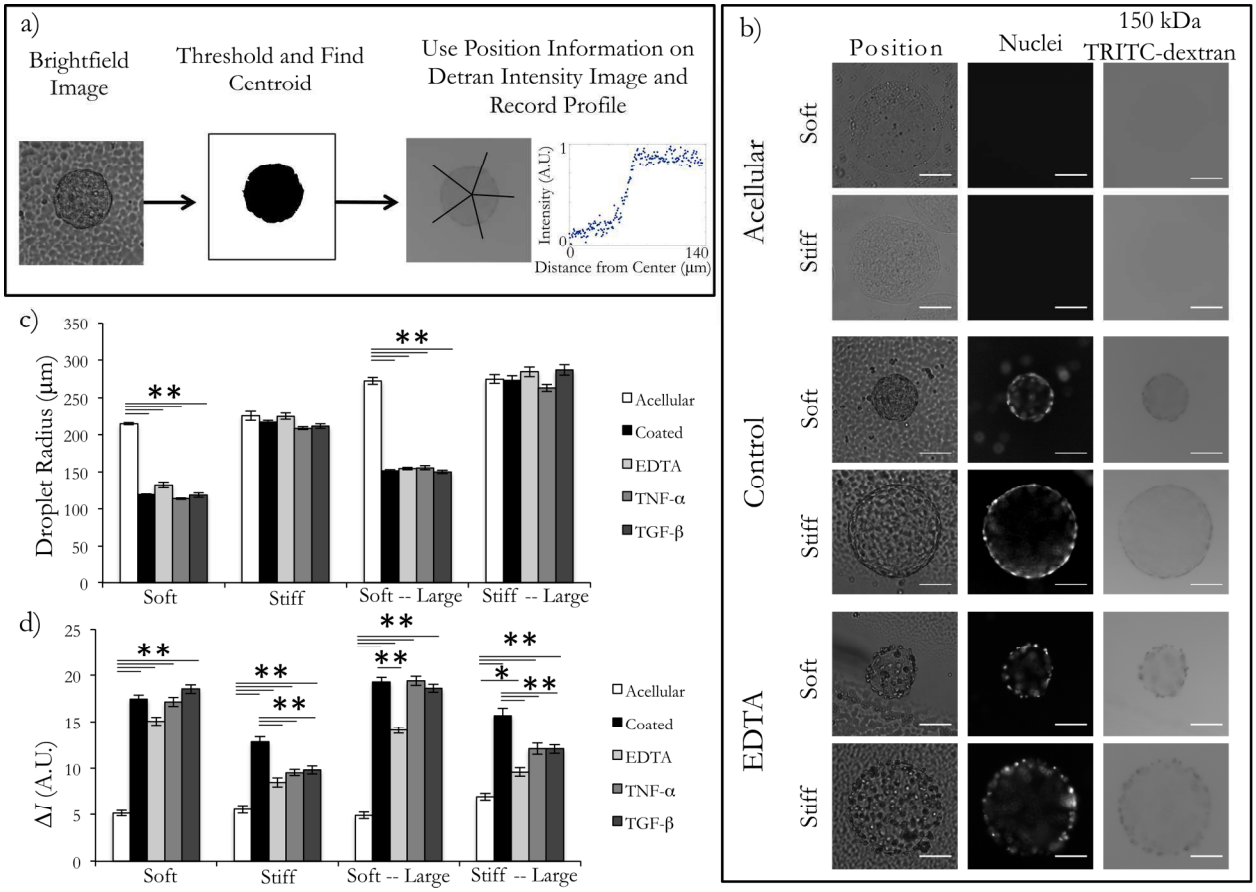

Figure 5: Endothelial barrier function can be assessed with widefield imaging for high throughput studies. Endothelial cells were cultured on the surface of collagen microtissues for 5 days before assessing permeability. Constructs were soaked in 12.5 ug/mL bath of 150 kDa fluorescent dextran. Constructs were then imaged with widefield microscopy for the brightfield and fluorescent channels. (a) To assess permeability, we used brightfield images to detect the centroid and edges of each microtissues and collected linescans from the center of the droplet to 100 pixels outside the edge of the construct. (b) Representative images from acellular, control HUEC-coated, and 5 mM EDTA treated microtissues are shown. (c) When comparing the average microtissue radius (shown with standard error) for each condition, we observed consistent compaction of soft microtissues, and little change in size of stiff microtissues. (d) To assess permeability, we calculated the difference in intensity between the outside and inside of the droplet (ΔI). We observed that the acellular constructs were more saturated with dye in all construct conditions for both sizes of dye. However, the cell monolayer demonstrated semi-permeable qualities, which was especially visible on the stiff constructs. We found the addition of the cell layer increased ΔI for all conditions ($p<0.01$). In the large-soft and both stiff conditions, the modulation of the cell layer with EDTA resulted in a statistically significant decrease in ΔI. When we tested inflammatory cytokines on our platform, TNF-α and TGF-β resulted in statistically signficant decreases in ΔI (relative to the coated control) for both sizes of stiff microtissues. From this, we concluded that the stiff microtissues were better suited for the macromolecular permeability assay (one-way ANOVA with post-hoc Tukey HSD test; $p<0.01$ = **, $p<0.05$ = *). Scale bars 100 μm.

Table of Contents Entry

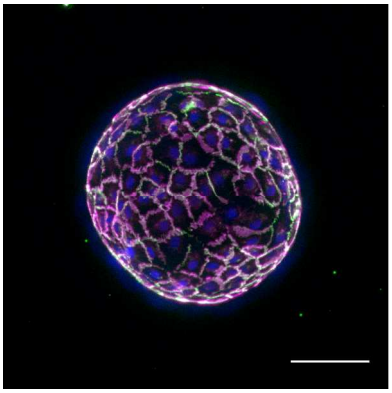

Using collagen microtissues, we show high-throughput assessment of endothelial function and permeability on natural ECM, supporting robust statistical analysis.